Detuning piezoelectric receivers by resistive load adjustment for electrodynamic wireless power transfer

Adrien Morel, Michael-Anas Dosol

Detuning piezoelectric receivers by resistive load adjustment for electrodynamic wireless power transfer

Adrien MOREL[1], **Michael-Anas DOSOL**[1]
[1] SYMME, Université Savoie Mont-Blanc, France

E-mail: adrien.morel@univ-smb.fr

Received xxxxxx
Accepted for publication xxxxxx
Published xxxxxx

Abstract

This article investigates electrical detuning techniques for low-frequency electrodynamic wireless power transfer (EWPT) systems. This study focuses on protecting the receiver from potential damage when quick increases in magnetic fields occur due to transmitter-receiver distance variation or in-rush transmitter coil currents. In the case of such event, to avoid damaging the mechanical receiver, the solution investigated in this article is to adjust the electrical load connected to the receiver. This adjustment enables precise tuning and detuning of the receiver's resonant frequency and damping characteristics, thereby allowing to reduce its mechanical displacement amplitude and protecting it from damage. Based on well-known models of EWPT systems, we develop an analysis of two key operational modes of the proposed tuning/detuning approach: Maximum Transmitted Power (MTP) mode, where the receiver circuitry's input impedance is optimized for peak power transfer, and Minimum Displacement (MD) mode, which involves electrically detuning the receiver's resonant frequency to limit its mechanical displacement. We establish transition conditions between MD and MTP modes based on the receiver voltage amplitude, enabling automated monitoring and adjustment of the receiver's detuning. Experimental validation has been conducted with an EWPT experimental setup and a custom piezoelectric receiver. The results, in good agreement with the proposed analytical model predictions, confirm the effectiveness of the proposed detuning algorithm, which successfully reduces the receiver displacement by 60% in response to sudden magnetic field increases.

Keywords: *Wireless power transfer, Electrodynamics, Electromechanical antenna, Detuning, Impedance matching, Resonance tuning, Piezoelectric material.*

Introduction

Implantable biomedical sensors and actuators (IBSA) have been extensively developed for modern medicine purposes, such as insulin pumps, glucose sensors, pacemakers, and artificial neurotransmitters [1]. Traditionally, these systems are powered by either implantable batteries or percutaneous links. However, batteries have a limited lifetime and require surgery to be replaced. Percutaneous links, on the other hand, carry a risk of infection and may pose some reliability issues. In recent decades, Wireless Power Transfer (WPT) has emerged as a promising alternative for powering implantable devices without requiring regular surgical operations and reducing the risk of infection [2].

Traditional WPT solutions are based on electromagnetic induction and magnetic resonance: an alternating current sent through a transmitter coil outside the human body generates an alternating magnetic field. The variation of the magnetic field induces an alternating voltage in the receiver coil located inside the human body. This voltage can be rectified to power the implanted device. Although inductive WPT technologies have been widely explored in the literature [3-5], their

operating frequency (typically 100 kHz – 10 MHz) presents several challenges:

- Significant absorption by conductive media, such as body fluids and the metallic shell around the supplied device, results in reduced transmission distance and power [6].
- Tissue heating from absorption of MHz magnetic fields might raise health concerns [7].
- An increased receiver size is needed to achieve lower resonant frequency [8].

An emerging solution, Electrodynamic Wireless Power Transfer (EWPT), has recently gained attention in the literature as a promising approach to address these issues [9,10]. Unlike inductive WPT, EWPT employs an electromechanical receiver with a much lower mechanical resonant frequency (10 Hz – 1000 Hz range), enabling a substantial reduction in the magnetic field frequency. Figure 1 illustrates an example of an EWPT system, where the transmitting coil generates a low-frequency (<1 kHz) magnetic field that is weakly absorbed by conductive media. This magnetic field drives a moving magnet attached to a mechanical resonator with a low resonant frequency that is tuned to the magnetic field frequency. Finally, the mechanical resonator's energy can be converted back into electrical energy using a piezoelectric material, which features relatively low conduction losses and occupies a small volume [11]. EWPT is particularly suited for biomedical applications, facilitating low-frequency power transfer without necessitating bulky receivers with compromised power density [12,13].

A common characteristic in biomedical applications is the variable coupling between the transmitter and receiver [14]. For instance, when the receiver is located in soft tissues, the coupling is likely to vary due to posture changes, contractions of the human body, breathing, and variations in the coils' orientation and distance. Such coupling variation might lead to sudden increases in the magnetic field at the receiver side, causing increased power dissipation, heating the tissues surrounding the receiver, and potentially damaging the implantable device. This challenge, well-known in the WPT community, has led to the development of various schemes [14-23] to protect the receiver and implantable device from increased magnetic fields and coupling variations. Some methods based on power electronics systems, like linear low dropout regulators (LDO), dissipate excess energy at the receiver side to maintain a constant voltage across the implantable device [15]. However, this approach still results in unwanted heat dissipation by the receiver circuitry. Alternative solutions based on the receiver's coil geometry and multi-degree-of-freedom moving-receiver solutions have also been explored to maintain a relatively constant coupling regardless of the receiver's orientation [16-18]. Additionally, some researchers have proposed detuning the resonant frequency of either the emitting [13, 19] or receiving [20] coil to regulate power flow. This has been achieved by connecting variable inductor circuits [21], soft switched capacitors [22], or LCL-network based current regulation schemes [23] to the receiver.

While all these approaches have been successfully developed for resonant inductive WPT systems, detuning techniques remain largely unexplored for EWPT. Detuning is however crucial for EWPT systems due to the mechanical nature of the electromechanical receiver, which must be safeguarded against potential damage from large magnetic fields and coupling strength variations. Traditional LDO-based solutions are unsuitable for EWPT as they do not reduce the mechanical energy within the receiver. Given the loose coupling between the receiver and emitter, a backward data transmission that could enable the direct control of the power sent via the transmitter seems intricate to implement. Moreover, the typically low power levels involved in EWPT systems (in the range of hundreds of μW to hundreds of mW) require a solution that is simple, miniaturized and self-powered.

Drawing inspiration from solutions in inductive WPT [14-23] and from known analysis made on linear piezoelectric harvesters [24-25], this paper proposes and evaluates a receiver-based electrical detuning approach for EWPT systems, specifically tailored to mitigate the risks associated with variable coupling. By adjusting the impedance of the circuit connected to the receiver, we demonstrate the ability to electrically adjust the resonance of the receiver, and match/unmatch it with the magnetic field frequency. Such approach can be used to either *tune* the receiver in Maximum Transmitted Power (MTP) mode, or *detune* it in Minimum Displacement (MD) mode.

This paper is structured as follows: the first section introduces models of the different parts of EWPT systems, providing the foundation for the analysis of the detuning scheme. The subsequent section details the proposed tuning/detuning mechanism and its theoretical framework. Lastly, we present and discuss experimental results validating the proposed detuning method with an EWPT setup.

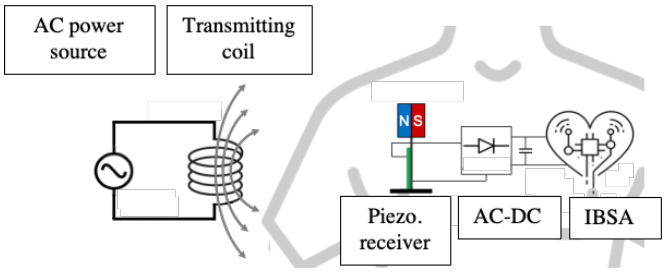

Figure 1 – System overview of an EWPT system.

Model of EWPT systems

This section describes the model of EWPT systems, such as the one illustrated in Fig.1. All the variables and notations

used throughout this paper are summarized in Table 1 for ease or reference.

Table 1: Variables and notations used in this manuscript

Part of the system	Var.	Meaning	Unit
Transmitting coil	I_{em}	Transmitter current	A
	$I_{em,m}$	Transmitter current amplitude	A
	N	Number of loops of the transmitting coil	-
	L	Coil's length	m
	D_e	Coil's external diameter	m
	D_i	Coil's internal diameter	m
	B	Magnetic field	T
	l	Transmitter-receiver distance	m
	χ_{em}	Current-field coupling coefficient	T/A
Receiver's magnet	V	Magnet volume	m³
	B_r	Magnet's remanent magnetic field	T
	χ_{rec}	Field-force coupling coefficient	N/T
Mechanical part of the receiver	F	Magnetic force	N
	F_m	Magnetic force amplitude	N
	x	Mass displacement	m
	x_m	Amplitude of the mass displacement	m
	$x_{m_{opt}}$	Optimal mass displacement for maximizing the transmitted power (MTP)	m
	$x_{m,lim}$	Limit mass displacement before damaging the receiver	m
	L_b	Receiver's beam length	m
	M	Receiver's mass	g
	K	Receiver's stiffness	N/m
	μ_m	Damping	N.m⁻¹.s
	$\omega_{0,m}$	Natural mechanical frequency	rad.s⁻¹
	ω	Angular frequency	rad.s⁻¹
	ω_{res}	Resonant frequency	rad.s⁻¹
	Ω_m	Dimensionless frequency	-
	Q	Receiver's quality factor	-
Receiver's piezoelectric material	α	Force factor	mN/V
	k_m^2	Squared expedient electromech. coupling	-
	C_p	Piezo. capacitance	nF
Electrical part of the receiver	R	Load resistance	Ω
	r	Dimensionless resistance	-
	v_p	Piezoelectric voltage	V
	$v_{p,m}$	Piezoelectric voltage amplitude	V
	i_p	Piezoelectric current	A
Universal constants	μ_0	Vacuum permeability	N.A⁻²
Mathematical notation	$\dot{f}$	Time derivative of f	-
	$\underline{f}$	Complex form of f	-

2.1 Magnetic Transmitter

The first part of the EWPT system is the transmitting coil that produces an low-frequency alternating magnetic field, as illustrated in Fig.2. From the Biot-Savart law, the expression of the magnetic field along the centerline of the coil produced by a solenoid with N loops can be derived [26, 27]:

$$B(l) = \frac{\mu_0 N\, I_{em}}{L\,(D_e - D_i)}\left[(L+l)\ln\left(\frac{h_1}{h_2}\right) + (-l)\ln\left(\frac{h_3}{h_4}\right)\right] \quad (1)$$

with I_{em}, L, D_e, and D_i being the coil current, the length of the coil, its external diameter, and its internal diameter, respectively. μ_0 is the vacuum permeability, and h_1, h_2, h_3 and h_4 are functions of solenoid geometry:

$$\begin{cases} h_1 = D_e + \sqrt{D_e^2 + (2L+2l)^2} \\ h_2 = D_i + \sqrt{D_i^2 + (2L+2l)^2} \\ h_3 = D_e + \sqrt{D_e^2 + (-2l)^2} \\ h_4 = D_i + \sqrt{D_i^2 + (-2l)^2} \end{cases} \quad (2)$$

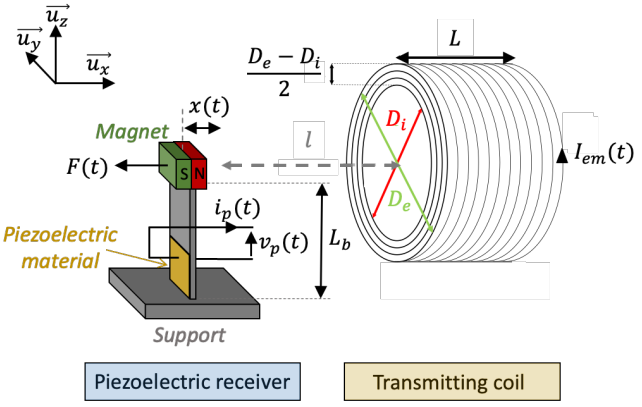

Figure 2 – Detailed illustration of the transmitting coil and the piezoelectric electromechanical receiver.

As shown by (1), the magnetic field is proportional to the coil current. Therefore, (1) can be rewritten as (3), with χ_{em} being a factor depending on the geometry of the transmitting coil and the transmitter–receiver distance.

$$B(l) = \chi_{em}(l)\, I_{em} \quad (3)$$

2.2 Electromechanical Receiver

The second part of the EWPT system is the electromechanical receiver. The receiver consists of a cantilever beam with glued piezoelectric materials and a magnetic inertial mass, as illustrated in Fig.2.

Due to the low-frequency magnetic field produced by the transmitting coil, a force F along the $\vec{u_x}$ direction is applied to the magnet. This force sets the cantilever beam in motion, which strains the piezoelectric material and induces a voltage v_p across it. This resonant system has been widely studied in the literature as a single-degree-of-freedom (SDoF) system

[24, 25], where both the mechanical resonator and the piezoelectric material behave linearly [28]. Although this linear assumption may be debatable in some cases [29], it remains reasonable as long as the mechanical displacement and voltage remain relatively limited [30].

Applying Newton's second law of motion and Khirchhoff's current law, the electromechanical equations governing the dynamics of the receiver are expressed as follows:

$$\begin{cases} F = M\ddot{x} + \mu_m \dot{x} + Kx + \alpha v_p \\ \alpha \dot{x} = C_p \dot{v_p} + i_p \end{cases} \quad (4)$$

where x, M, μ_m, K, and α represent the mechanical displacement in $\overrightarrow{u_x}$ direction (perpendicular to the beam length), the inertial mass, the mechanical damping, the stiffness, and the force factor of the receiver, respectively. C_p is the capacitance of the piezoelectric material, and i_p is the current drawn from the electrical circuit connected to the piezoelectric material.
The magnetic force F can be expressed as a function of the magnetic field B, assuming that the transmitter magnetic field is aligned with the magnet internal field [27]:

$$F(t) = \frac{V\, B_r}{L_b\, \mu_0} B(t) = \chi_{rec}\chi_{em}\, I_{em}(t) \quad (5)$$

where V and B_r are the magnet volume and remanent field, respectively. L_b is the length of the cantilever beam, and $\chi_{rec} = \frac{V\, B_r}{L_b\, \mu_0}$ is a factor depending on the geometry of the receiver. Using equations (4) and (5), the dynamics of the receiver can be computed for any current waveforms in the transmitting coil.

2.3 System-level considerations

Figure 3 illustrates energy transmission in EWPT systems, along with a circuit model based on equations (4) and (5). From the circuit model from Fig.3 and based on impedance matching theory, the maximum power that can be transmitted to the receiver circuitry is given by (6).

$$P_{max} = \frac{F_m^2}{8\mu_m} = \frac{\left(\chi_{rec}\chi_{em}\, I_{em,m}\right)^2 Q}{8\, M\, \omega_{0,m}} \quad (6)$$

where F_m is the amplitude of the magnetic force, $Q = \sqrt{KM}/\mu_m$ is the quality factor of the mechanical receiver, and $\omega_{0,m} = \sqrt{K/M}$ is its natural mechanical frequency. This maximum power is achieved if the electromechanical receiver operates at resonance and if the energy harvested by the circuit is equal to the dissipated energy in the mechanical damper ($\alpha \int_0^T v_p \dot{x} dt = \mu_m \int_0^T \dot{x}^2 dt$).

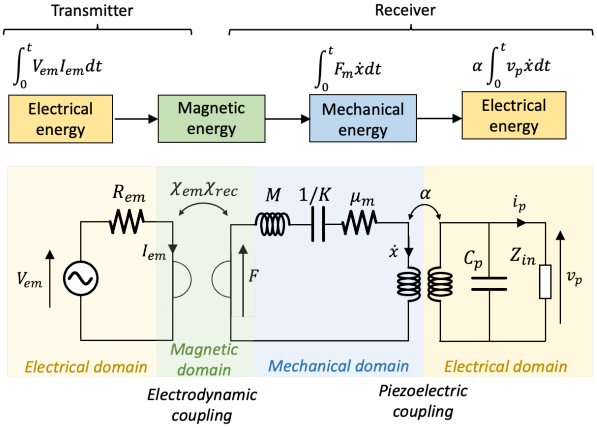

Figure 3 – Energy chain and circuit model of a standard EWPT system [11] with piezoelectric electromechanical transduction. Z_{in} represents the input impedance of the receiver circuitry.

Equation (6) demonstrates that a larger transmitter-receiver coupling $\chi_{rec}\chi_{em}$ leads to greater maximum transmitted power. However, if this coupling becomes excessively large, (i.e., if the magnetic transmitter suddenly moves closer to the receiver due to breathing or posture change), the mechanical displacement of the receiver will increase, potentially leading to damage.

Building on the models developed in this section, the next section will provide an analytical analysis of the impact of the electrical circuit, focusing on either maximizing the transmitted power or protecting the receiver from damage.

Operating modes: power transfer and detuning

3.1 Maximum Transmitted Power (MTP) mode

To maximize the transmitted power, the input impedance of the receiver circuitry must be adapted and optimized. In the following, this operation mode is referred to as *Maximum Transmitted Power* (MTP) mode. Considering that the input impedance of the circuit is resistive[1], the second equation of (4) can be written as follows in the complex domain:

$$\alpha\, j\, \omega\, \underline{x} = j\, \omega\, C_p \underline{v_p} + \frac{\underline{v_p}}{R} \quad (7)$$

where R is the input resistance of the electrical circuit. The notation $\underline{x}$ and $\underline{v_p}$ represent the complex versions of the variables x and v_p, respectively. Rearranging the terms in (7) yields the following expression for the piezoelectric voltage in the complex domain:

[1] As a matter of example, this is the case for a full diode bridge followed by a DC-DC converter with no filtering capacitor [31].

$$\underline{v_p} = \frac{\alpha \underline{x}}{C_p}\left[\frac{(r\Omega_\mathrm{m})^2}{1+(r\Omega_\mathrm{m})^2} + j\frac{(r\Omega_\mathrm{m})}{1+(r\Omega_\mathrm{m})^2}\right] \quad (8)$$

where $r = RC_p\omega_{0,m}$ is the normalized load resistance, and $\Omega_m = \omega/\omega_{0,m}$ is the normalized vibration frequency. Injecting this expression into the first equation of (4) rewritten in the complex domain leads to the expression of the displacement $\underline{x}$, (9).

$$\underline{x} = \frac{\chi_{rec}\chi_{em}\,\underline{I_{em}}}{\left(K - M\omega^2 + \frac{\alpha^2}{C_p}\frac{(r\Omega_\mathrm{m})^2}{1+(r\Omega_\mathrm{m})^2}\right) + j\left(D\omega + \frac{\alpha^2}{C_p}\frac{(r\Omega_\mathrm{m})}{1+(r\Omega_\mathrm{m})^2}\right)} \quad (9)$$

Rearranging the terms, (9) can be rewritten with physical dimensionless quantities:

$$\underline{x} = \frac{\chi_{rec}\chi_{em}\,\underline{I_{em}}/K}{\left(1 - \Omega_\mathrm{m}^2 + k_m^2\frac{(r\Omega_\mathrm{m})^2}{1+(r\Omega_\mathrm{m})^2}\right) + j\left(\frac{\Omega}{Q} + k_m^2\frac{(r\Omega_\mathrm{m})}{1+(r\Omega_\mathrm{m})^2}\right)} \quad (10)$$

where $k_m^2 = \alpha^2/(KC_p)$ is the squared expedient coupling of the receiver. From (10), the amplitude of the mechanical displacement can be found:

$$x_m = \frac{\chi_{rec}\chi_{em}\,I_{em,m}/K}{\sqrt{\left(1 - \Omega_\mathrm{m}^2 + \frac{k_m^2\,(r\Omega_\mathrm{m})^2}{1+(r\Omega_\mathrm{m})^2}\right)^2 + \left(\frac{\Omega_\mathrm{m}}{Q} + \frac{k_m^2\,(r\Omega_\mathrm{m})}{1+(r\Omega_\mathrm{m})^2}\right)^2}} \quad (11)$$

From (11), the expression of the harvested power can also be found, which is very similar to the one obtained for piezoelectric energy harvesters [25]:

$$P = \frac{4k_m^2\Omega_\mathrm{m}\frac{P_{max}}{Q}\frac{(r\Omega_\mathrm{m})}{1+(r\Omega_\mathrm{m})^2}}{\left(1 - \Omega_\mathrm{m}^2 + k_m^2\frac{(r\Omega_\mathrm{m})^2}{1+(r\Omega_\mathrm{m})^2}\right)^2 + \left(\frac{\Omega_\mathrm{m}}{Q} + k_m^2\frac{(r\Omega_\mathrm{m})}{1+(r\Omega_\mathrm{m})^2}\right)^2} \quad (12)$$

In MTP mode, the resistance needs to be optimized in order to maximize the transmitted power. Figure 4 shows the evolution of the transmitted power (with optimized magnetic field frequency), as a function of the figure of merit of the receiver (i.e., $k_m^2 Q$, the product of its coupling k_m^2 and its quality factor Q). As illustrated in Fig.4, the optimal resistance depends on the receiver's coupling, and needs to be optimized to maximize the transmitted power. When $k_m^2 Q > 2$, the maximum power P_{max} can be achieved. For larger values of $k_m^2 Q$, a bifurcation of the optimal resistance is observed, with two optimal resistances corresponding to two distinct transmission frequencies.

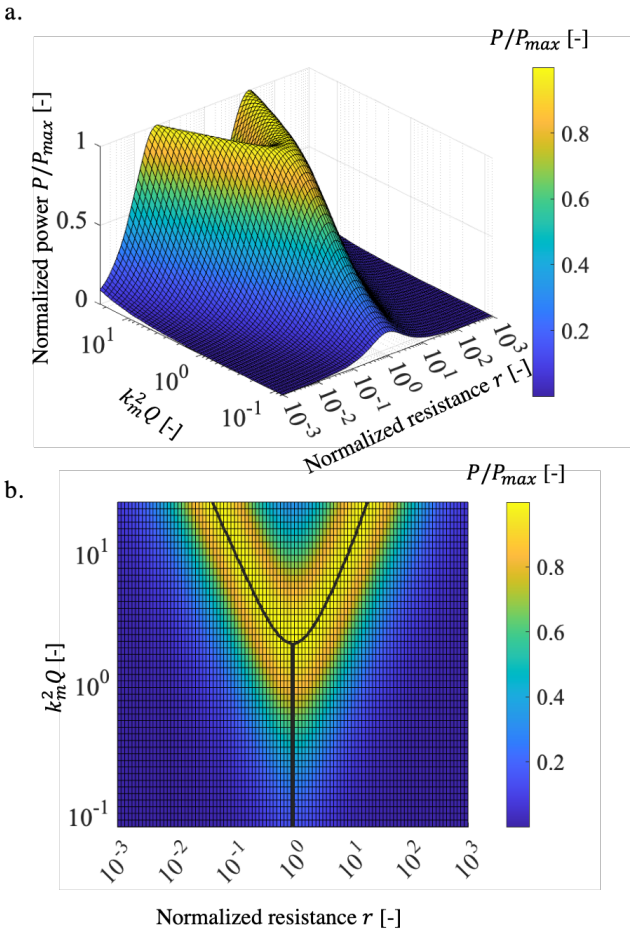

Figure 4 – a. 3D and b. 2-D view of the transmitted power as a function of the normalized resistance of the circuit r and the figure of merit $k_m^2 Q$ of the electromechanical receiver. The black line highlights the maximized transmitted power with optimal normalized resistance r_{opt}.

As already proven for linear piezoelectric energy harvesters [25,33], the expressions for the optimal resistance and optimal transmission frequency for maximizing the transmitted power are expressed analytically in (13) and (14), respectively.

$$r_{opt} = \frac{1}{\Omega_\mathrm{m}}\sqrt{\frac{\Omega_\mathrm{m}^2 + Q^2(1-\Omega_\mathrm{m}^2)^2}{\Omega_\mathrm{m}^2 + Q^2(k_m^2 + 1 - \Omega_\mathrm{m}^2)^2}} \quad (13)$$

$$\Omega_{opt} = \frac{1}{Q}\sqrt{Q^2\left(1 + \frac{k_m^2}{2}\right) - 1 \pm \sqrt{(1 - Q^2k_m^2)^2 - 4Q^2}} \quad (14)$$

Equations (13) and (14) show that either one or two optimal pairs (r, Ω_m) exist for maximizing power. If $k_m^2 Q > 2$ (as is typically the case for most modern piezoelectric receivers), these expressions can be simplified as follows:

$$\text{Case (1):} \begin{cases} r_{opt,1} \approx \frac{1}{\sqrt{1+(k_m^2 Q)^2}} \\ \Omega_{opt,1} \approx 1 \end{cases} \qquad \text{Case (2):} \begin{cases} r_{opt,2} \approx \frac{\sqrt{1+k_m^2+(Qk_m^2)^2}}{1+k_m^2} \\ \Omega_{opt,2} \approx \sqrt{1+k_m^2} \end{cases} \tag{15}$$

The first combination of optimal solutions $(r_{opt,1}, \Omega_{opt,1})$ corresponds to a resonance close to the short-circuit resonance of the receiver, associated with a relatively small resistive load (left branch in Fig.4). The second solution $(r_{opt,2}, \Omega_{opt,2})$ corresponds to a resonance close to the open-circuit resonance of the receiver, associated with a relatively large resistive load (right branch in Fig.4). One of these two conditions (15) must be fullfilled to maximize the transmitted power. If the power is maximized ($P = P_{max}$), the expression for the displacement amplitude is given by equation (16):

$$x_{m_{\text{opt}}} = \frac{Q\, \chi_{rec}\chi_{em}\, I_{em}/K}{\sqrt{2}\Omega_{\text{m}}} \tag{16}$$

3.2 Minimum Displacement (MD) mode

In various practical scenarios, the displacement amplitude of the mechanical receiver may experience sudden increases. In the context of biomedical applications, this could result, for instance, from coupling variations due to breathing and posture changes, leading to a sudden increase in the magnetic field and thus in the receiver's motion amplitude. Since the receiver is a mechanical resonator, its displacement amplitude is directly related to the stress in the piezoelectric and substrate materials. Consequently, the displacement amplitude of the receiver should not exceed a limit, denoted as $x_{m,lim}$, to ensure that the stress in the substrate and piezoelectric materials remains below the yield stress [34, 35]. Note that the relation between maximum displacement amplitude and yield stress depends on the receiver's geometry and materials. This receiver-specific relationship is not detailed in this paper but is discussed in various literature sources [36, 37].

If $x_m > x_{m,lim}$, it becomes imperative to stop transmitting energy and instead safeguard the mechanical receiver to prevent damage caused by excessive displacement. In this study, we refer to this operational mode as the *Minimum Displacement* (MD) mode. Three solutions can be investigated to bound the mechanical displacement:

- Limiting the electrical energy sent in the transmitter
- Limiting the magnetic field seen by the receiver
- Limiting the mechanical energy within the receiver

Constraining the transmission of energy from the transmitter can be accomplished; however, establishing a feedback mechanism between the transmitter and receiver may not be readily achievable and could be a challenge due to the weak transmitter-receiver coupling. Similarly, limiting the magnetic field perceived by the receiver can be intricate, as it may necessitate active shielding techniques that could require considerable volume. Ultimately, limiting the mechanical energy within the receiver by detuning the receiver resonant frequency is feasible with simple low-power electronics without requiring transmitting data from the receiver to the transmitter. This section proposes to explore this solution through the adjustment of the electrical load.

Combining (11) with (15), it is possible to evaluate the displacement amplitude that can be obtained by adjusting the resistive load connected to the piezoelectric material:

$$\frac{x_m(r)}{x_{m_{opt}}} = \frac{2\,\Omega_{\text{m}}/Q}{\sqrt{\left(1-\Omega_{\text{m}}^2+\frac{k_m^2\,(r\Omega_{\text{m}})^2}{1+(r\Omega_{\text{m}})^2}\right)^2+\left(\frac{\Omega_{\text{m}}}{Q}+\frac{k_m^2\,(r\Omega_{\text{m}})}{1+(r\Omega_{\text{m}})^2}\right)^2}} \tag{17}$$

If the receiver is weakly coupled ($k_m^2 Q \leq 2$), the displacement cannot be further reduced, meaning that $min\left(\frac{x_m(r)}{x_{m_{opt}}}\right) = 1$. If the receiver is strongly coupled ($k_m^2 Q > 2$), which is the case for most modern piezoelectric receivers [37, 38], two cases can be considered depending on which condition (15) is fulfilled in MTP mode for maximizing the transmitted power.

Figure 5.a shows the evolution of the relative displacement for these two cases. The blue curve illustrates the evolution of x_m/x_{opt} when the MTP frequency and resistance are $\Omega_{opt,1} = 1$ and $r = r_{opt,1}$. In this case, decreasing the resistance tends to increase the mechanical displacement, while increasing the resistance decreases it. Conversely, the red curve illustrates the evolution of x_m/x_{opt} for $\Omega_{opt,2} = \sqrt{1+k_m^2}$ and $r = r_{opt,2}$. Here, decreasing the resistance reduces the mechanical displacement, while increasing the resistance increases it.

This behavior can be explained by analyzing the impact of the resistance on the receiver's resonance frequency, ω_{res}. The expression of the receiver's resonant frequency ω_{res} can be approximated by (18), as detailed in Appendix A.

$$\Omega_{res} \approx \frac{1}{r}\sqrt{\frac{(r^2(1+k_m^2)-1)+\sqrt{(r^2(1+k_m^2)-1)^2+4r^2}}{2}} \tag{18}$$

With $\Omega_{res} = \omega_{res}/\omega_{0,m}$ being the dimensionless resonant frequency of the receiver. Equation (18) and Fig.5.b show that if the short-circuit resonance is used in MTP mode (case 1), detuning the receiver to limit its mechanical energy can be achieved by increasing the resistance, which raises the resonance frequency (up to the open-circuit resonance frequency). If the open-circuit resonance is used in MTP mode (case 2), detuning the harvester can be achieved by decreasing the resistance, lowering the resonance frequency (down to the short circuit resonance frequency).

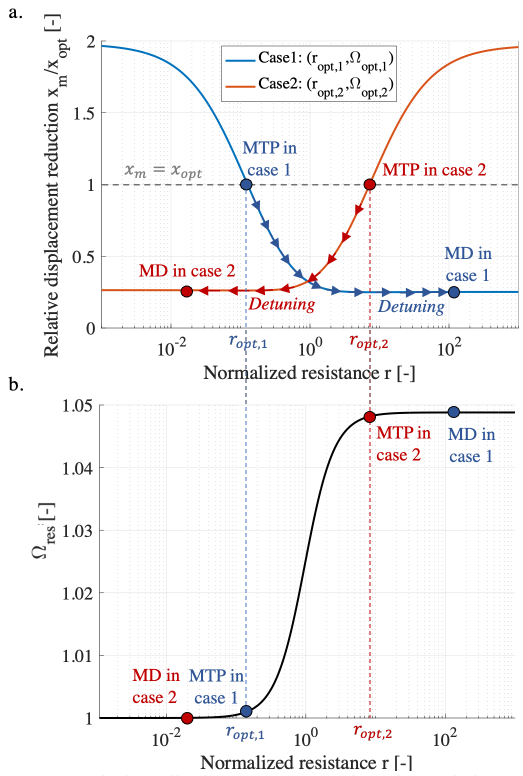

Figure 5 – Relative displacement as a function of the normalized resistance, depending on the initial optimal conditions for maximizing the transmitted power (15). For this simulation, $k_m^2 = 0.1$ and $Q = 80$.

The minimum relative displacement in case 1 ($\Omega_{opt,1} = 1$) can be calculated by considering a large resistive load to minimize the displacement:

$$\min\left(\frac{x_m(r)}{x_{m_{opt}}}\right) = \frac{x_m(r \to +\infty)}{x_{m_{opt}}} = \frac{2}{\sqrt{(k_m^2 Q)^2 + 1}} \tag{19}$$

Similarly, in case 2 ($\Omega_{opt,2} = \sqrt{1 + k_m^2}$), the minimum relative displacement can be calculated by considering a small resistive load:

$$\min\left(\frac{x_m(r)}{x_{m_{opt}}}\right) = \frac{x_m(r \to 0)}{x_{m_{opt}}} = \frac{2}{\sqrt{\frac{(k_m^2 Q)^2}{1 + k_m^2} + 1}} \tag{20}$$

For the receiver used in Fig.5 ($k_m^2 = 0.1$, $Q = 80$), equations (19) and (20) yield a minimum relative displacement of approximately 0.25, as confirmed by the numerical result shown in Fig.5.a.

Both equations (19) and (20) prove that the minimum relative displacement depends only on the electromechanical coupling and quality factor of the receiver. The greater the electromechanical coupling, the more significant the impact of the electrical load on shifting the receiver's resonant frequency, as illustrated by (19) and Fig.5.b. The larger the quality factor, the greater the impact a small frequency shift has on the displacement amplitude. One may note that the minimum relative displacement in case 2 is always larger than in case 1. Therefore, our analysis will focus on case 1, which is more pertinent in MD, but also in MTP because it is less sensitive to dielectric losses in the receiver due to the smaller optimal voltage [39].

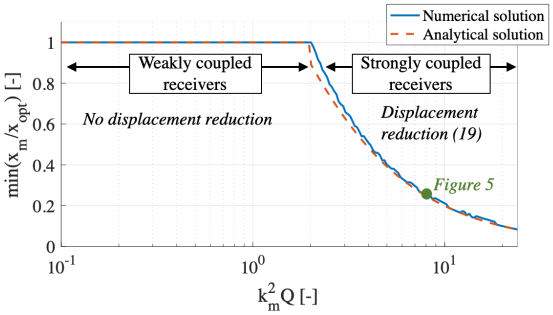

Figure 6 – Minimum relative displacement as a function of the coupling-quality factor product of the receiver, $k_m^2 Q$.

Figure 6 illustrates the evolution of the minimum relative displacement as a function of the coupling-quality factor product ($k_m^2 Q$) of the receiver. The analytical solution corresponds to equation (19) while the numerical solution is obtained by numerically solving the EWPT dynamic equations (1), (4) and (5) using Matlab Simulink. The good agreement between the analytical model and the numerical results confirms the validity of the proposed analytical equations for estimating the detuning capability of a given receiver.

Figure 6 also shows that weakly coupled receivers ($k_m^2 Q \leq 2$) cannot operate in MD mode, as their displacement cannot be reduced by electrical means. Conversely, for strongly coupled receivers ($k_m^2 Q > 2$), a higher $k_m^2 Q$ results in improved MD mode performance. For example, a strongly coupled receiver such as the one introduced in [37] ($k_m^2 Q = 26$) enables a maximum displacement reduction of 92.3%. As detailed in Appendix B, a stronger electromechanical coupling allows for the use of this detuning approach over a broader range of magnetic field amplitudes.

3.3 Transition conditions between MD and MTP modes

To automatically transition from MD to MTP mode, and vice-versa, it is necessary to identify analytical conditions on the receiver voltage that indicate when the receiver displacement is too large (requiring a shift to MD), and when it is sufficiently low (allowing a return to MTP).

From equation (8), the piezoelectric voltage amplitude $v_{p,m}$ is shown to be related to the mechanical displacement amplitude , x_m, by the following expression:

$$x_m = v_{p,m} \frac{C_p}{\alpha} \frac{\sqrt{1 + (r\Omega_m)^2}}{r\Omega_m} \tag{21}$$

From equations (21) and (15), the relationship between x_m and $v_{p,m}$ can be found in MTP mode (case 1).

$$x_m|_{MTP} = v_{p,m}|_{MTP} \frac{C_p}{\alpha} \sqrt{2 + (k_m^2 Q)^2} \quad (22)$$

From (22), a condition on the maximum value of $v_{p,m}$ can be established to limit the displacement of the receiver below a limit amplitude, $x_{m,lim}$.

$$v_{p,m}|_{MTP} > \frac{\alpha}{C_p} \frac{x_{m,lim}}{\sqrt{2 + (k_m^2 Q)^2}} \quad (23)$$

Similarly, a condition on the voltage can be established to ensure that the system can transition from MD to MTP mode while keeping the displacement amplitude below $x_{m,lim}$. Considering that the electrical load is disconnected in MD (i.e., $R \to \infty$), the mechanical displacement amplitude in MD is linked to the voltage amplitude by:

$$x_m|_{MD} = \frac{C_p}{\alpha} v_{p,m}|_{MD} \quad (24)$$

Combining the relationship between the displacement amplitude in MD mode (19) and the displacement amplitude in MTP mode (24), we find the expression of the mechanical displacement after switching from MD to MTP mode:

$$x_m|_{MTP} = \frac{\frac{C_p}{\alpha} v_{p,m}|_{MD}}{\left(\frac{x_m(r \to +\infty)}{x_{m_{opt}}}\right)} = \frac{C_p}{2\alpha} v_{p,m}|_{MD} \sqrt{(k_m^2 Q)^2 + 1} \quad (25)$$

Since this displacement has to be smaller than x_{lim}, it provides another condition that must be met to transition safely from MD to MTP:

$$v_{p,m}|_{MD} < \frac{2\alpha\, x_{m,lim}}{\sqrt{(k_m^2 Q)^2 + 1}\, C_p} \quad (26)$$

Equations (23) and (26) constitute the transition conditions on the piezoelectric voltage, allowing the switch from MTP to MD when the displacement becomes too large, and from MD to MTP when the displacement is sufficiently low.

Based on equations (23) and (26), Fig. 7 illustrates an algorithm for transitioning between MTP and MD modes to avoid breaking the receiver. When the system operates in MTP mode, the resitive load is fixed to its optimal value (15) to maximize the transmitted power. As long as (23) is not satisfied, it indicates that the displacement amplitude of the receiver is below the displacement amplitude threshold, $x_{m,lim}$. If (23) is satisfied (i.e., if $x_m > x_{m,lim}$), the system immediately enters MD mode to detune the receiver and decrease its displacement. In MD mode, the piezoelectric material is left in an open-circuit condition ($r \to \infty$) by disconnecting the harvesting circuit from the piezoelectric material.

Such algorithm is an exemple of a function that could be implemented in the receiver circuitry, in order to protect the receiver. The experimental validation of such algorithm is detailed in section 4.3.

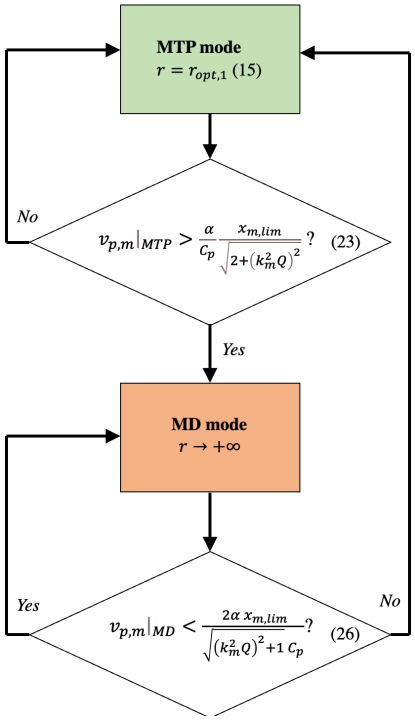

Figure 7 – Flowchart of the proposed algorithm for automated transition between MTP and MD operation modes.

While the detuning approach proposed in this section is relatively simple, it does not enable the maximization of transmitted power in MD mode, due to the null power in open-circuit condition. An optimal detuning mode that maximizes transmitted power is detailed in Appendix C, illustrating the maximum power achievable with this detuning approach through fine-tuning of the resistive load.

Experimental results

4.1 Experimental setup

To validate the theory behind the proposed electrical MD mode and the transition between MTP and MD modes, we developed an experimental setup for the EWPT system. This setup is shown in Fig.8.a and illustrated in Fig. 8.b.

The testbench has been automated using dSpace, wherein the dSpace console controls a DC-AC converter responsible for powering the transmitting coil. The transmitter consists of commercial Helmholtz coils 3B Scientific 1000906, with a single coil used as the transmitter. The parameters of this coil are summarized in Table 2.

The receiver comprises a steel cantilever beam coated with two PZT material plates (Fig.8.c). Additionally, the tip mass of the receiver consists in two 28g neodymium magnets. The piezoelectric plates are connected to a programmable decade resistance box, adjustable from the dSpace platform. Both

voltage and mechanical displacement waveforms are monitored using a custom voltage follower and fiber laser vibrometer.

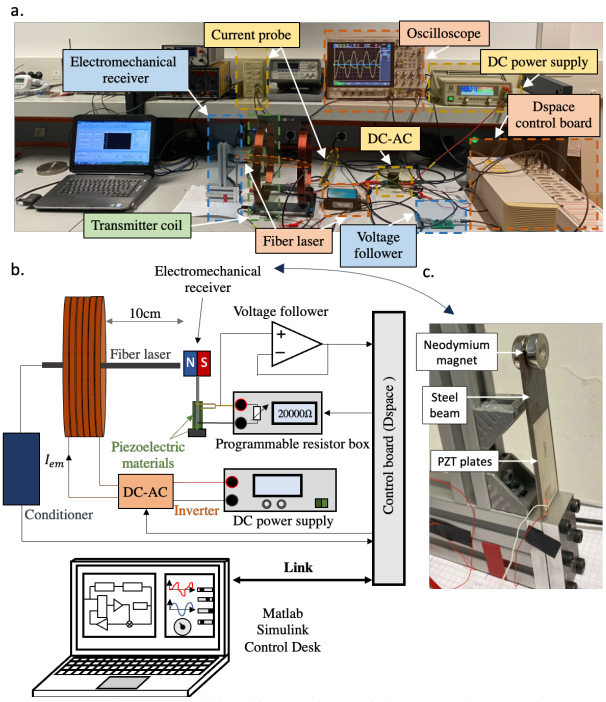

Figure 8 – a. Picture and b. Illustration of the experimental setup of the EWPT system for validation of MTP and MD operation modes and c. electromechanical receiver used during the experiments.

The electromechanical receiver shown in Fig.8.c. has been fabricated and characterized. Its mechanical natural frequency ω_0, quality factor Q, piezoelectric capacitance C_p and expedient electromechanical coupling k_m^2 were identified with an impedance analyzer, following the methodology outlined in [40]. The receiver's admittance measured from the piezoelectric electrodes was matched with an analytical model to determine $\omega_{0,m}$, Q, C_p, k_m^2, with a fitting algorithm in Matlab. The value of the inertial mass M was directly measured based on the weights of the receiver's tip magnets. The value of quality factor was recalibrated through frequency response measurements of the receiver and by matching them with theoretical model (11), under a 4A transmitter current amplitude. This adjustment provided a more precise estimate of Q considering its decrease under large mass displacement due to mechanical nonlinearities under moderate and high excitations. The values for stiffness $K = \omega_{0,m}^2 M$, damping $\mu_m = \sqrt{KM}/Q$, force factor $\alpha = \sqrt{k_m^2 K C_p}$ were deduced from the other parameters. The obtained parameters of the piezoelectric receiver are summarized in Table 3.

4.2 Power and displacement mapping

The EWPT system has been characterized with the automated dSpace testbench shown in Fig. 8, for a transmitter coil current of 4A and a transmitter-receiver distance of 10cm. The transmitted power in the resistive load connected to the receiver has been measured, for 60 frequencies between 33.5Hz and 36.5Hz, and for 60 load resistance values between 100Ω and 4MΩ. The results are shown in Fig.9.

Table 2: Parameters of the transmitting coil

Var.	Definition	Values	Units
N	Number of loops of the transmitting coil	124	-
L	Coil's length	25	mm
D_e	Coil's external diameter	311	mm
D_i	Coil's internal diameter	287	mm

Table 3: Parameters of the piezoelectric receiver

Var.	Definition	Values	Units
M	Mass	60	g
K	Stiffness	1900	N/m
μ_m	Damping	0.1	N/(m.s^{-1})
α	Force factor	5.3	mN/V
C_p	Piezo. capacitance	314	nF
$\omega_{0,m}$	Mechanical natural frequency	218	rad.s^{-1}
Q	Quality factor	131	-
k_m^2	Expedient electromech. coupling	0.046	-

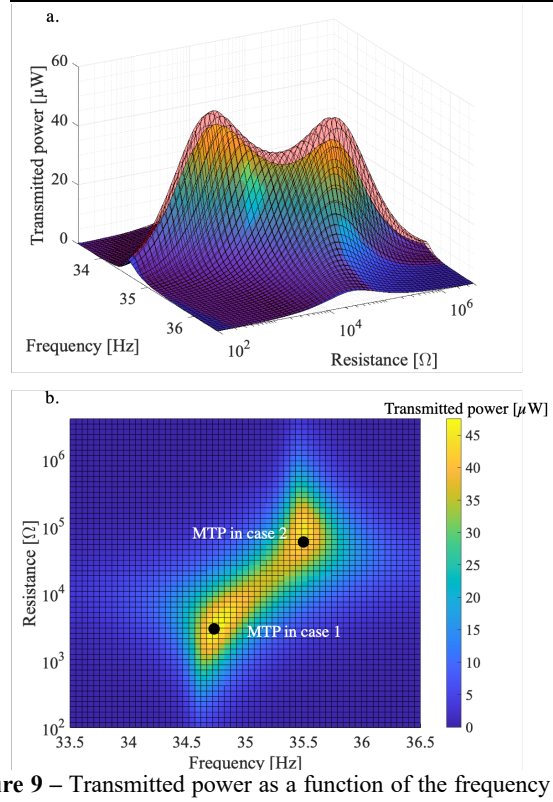

Figure 9 – Transmitted power as a function of the frequency of the transmitter coil current and resistance of the receiver load. a. Comparison of analytical model (red surface) with experimental measurements (colored surface), and b. top view of the experimental measurements. The transmitter-receiver distance is 10cm, and the amplitude of transmitter coil current is 4A. Note that the red surface has been lifted by 5% to enhance visibility.

As shown in Fig.9.a, the analytical model (equation (12)) is in good agreement with the experimental measurements, confirming the validity of the model and analysis. Due to the relatively strong $k_m^2 Q$ of the receiver ($k_m^2 Q \approx 6 > 2$), the power surface admits two maxima, for two (frequency-resistance) couples, which are related to cases 1 and 2 previously defined in this paper (15). The maximum power that can be transmitted is 45µW, and strongly depends on the transmitter-receiver distance and transmitter coil current (6).
Figure 10 shows the measurements of the receiver displacement amplitude, as a function of the resistance and frequency. As shown in Fig.10, there are two areas where the displacement amplitude is significant (220µm):

- around the short-circuit resonant frequency (34.8 Hz) when the resistance is low
- around the open-circuit resonant frequency (35.5 Hz) when the resistance is high

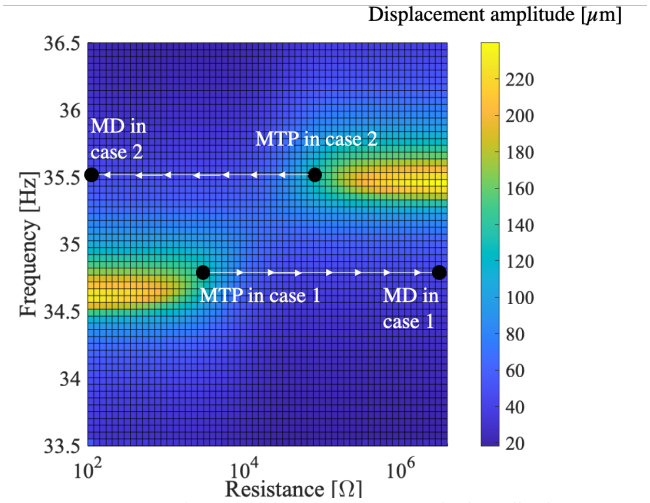

Figure 10 – Experimental measurements of the displacement amplitude of the electromechanical receiver, as a function of the frequency of the transmitter coil current and resistance of the receiver load. The transmitter-receiver distance is 10cm, and the amplitude of the transmitter coil current is 4A.

The MTP modes (corresponding to the power maxima in Fig.9) are shown in Fig.10, and correspond to relatively large displacement amplitudes (145µm). To transistion from MTP mode to MD mode, detuning of the resonant frequency is obtained by adjusting the resistive load value. As illustrated in Fig.10, when the system operates in MTP around the short-circuit resonant frequency (case 1), increasing the resistance can decrease the displacement amplitude. In the other hand, when the system operates in MTP around the open-circuit resonant frequency (case 2), decreasing the resistance can reduce the displacement amplitude.

Figure 11.a depicts the evolution of the relative displacement ratio $x_m/x_{m_{opt}}$ for both MTP cases (short-circuit and open-circuit resonances). The data show that with the receiver in Fig.8, it is possible to achieve a 67% decrease in displacement in case 2, and a 68.2% decrease in case 1. These measurements are in good agreement with the analytical models (equations (19) and (20)), although some discrepancies are observed when the receiver motion becomes large ($x_m > 1.4\, x_{opt}$). These discrepencies are attributed to damping and stiffness nonlinearities of the receiver that arise under large motions. It is important to note that these nonlinearities do not affect the relationship between displacement and voltage, and therefore, do not impact the transition condition developed in section 3.3.

Figure 11.b shows the evolution of the receiver's resonant frequency as a function of the resistance. Although the frequency range for tuning the resonant frequency is relatively limited (from 34.6 Hz to 35.5 Hz), due to the moderate coupling of the receiver, even a small mismatch between the magnetic field frequency and resonant frequency can lead to a significant decrease in motion.

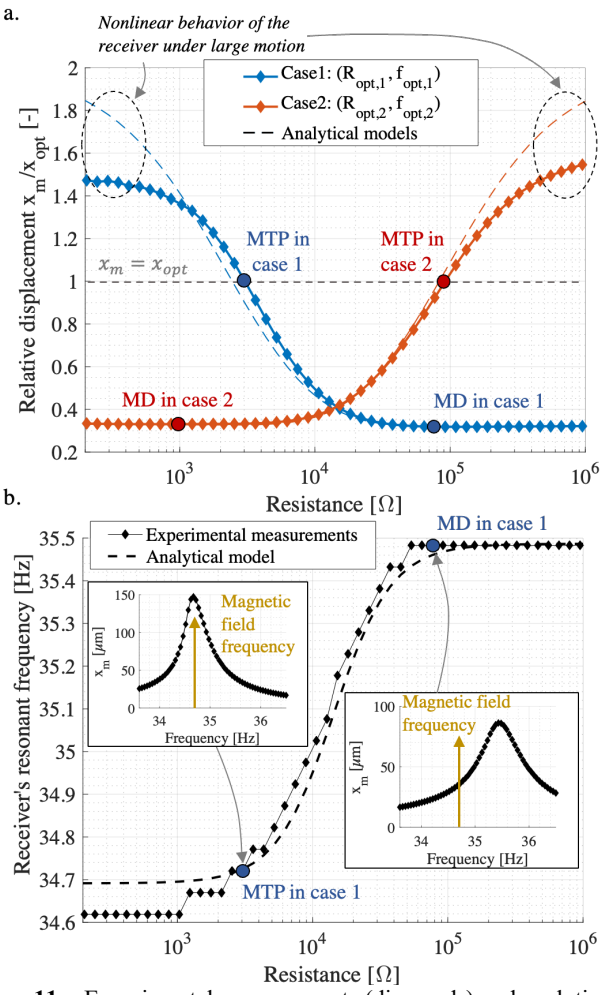

Figure 11 – Experimental measurements (diamonds) and analytical models (dashed lines) illustrating the impact of the load on the receiver's a. displacement amplitude, and b. resonant frequency.

4.3 Validation of the automated detuning mode

In this section, we aim to validate the automated transition between MD and MTP modes, based on the algorithm shown in Fig.7. This algorithm has been implanted on dSpace: when the receiver voltage amplitude exceeds $v_{p,m}|_{MTP}$ (23), the dSpace console sends a signal to a MOS transistor, which disconnects the resistive load from the receiver. Consequently, the receiver is in open-circuit condition ($r \to \infty$) and is detuned (MD mode). If the voltage amplitude drops below $v_{p,m}|_{MD}$ (26), the system determines that the mechanical displacement is sufficiently low and transitions back to MTP.

Figure 12 depicts the receiver's displacement as a function of time, illustrating the operation of the automated detuning algorithm. Initially, the receiver is placed at a distance of 10cm from the transmitting coil and operates in MTP mode, with the transmitting coil powered by a current of amplitude 2A. At $t = 9s$, the magnetic field is rapidly increased (by increasing the amplitude of transmitter coil current from 2A to 4A), leading to a sudden increase in mechanical displacement. When the mechanical displacement exceeds $x_{m,lim}$ =100µm (set as the displacement limit for this experiment, which corresponds to approximately 25% of the PZT's limit stress for our receiver [34]), the receiver voltage consequently exceeds $v_{p,m}|_{MTP}$. As a result, the dSpace console disconnects the resistive load from the receiver (MD mode). In MD mode, the displacement quickly decreases, stabilizing at an amplitude of 58µm, well below the displacement limit. At $t = 21s$, the amplitude of the transmitter coil current is reduced back to 2A, decreasing the mechanical displacement of the receiver. Since $v_p < v_{p,m}|_{MD}$, the dSpace console reconnects the resistive load to the receiver, and the system returns in MTP mode. The mechanical displacement amplitude then increases back to an amplitude of 80µm.

Figure 13 presents the evolution of the mechanical displacement as a function of time when the detuning system is deactivated. When the magnetic field is increased, the mechanical displacement also increases, leading to a mechanical displacement of 145μm, which exceeds x_{lim}. Figures 12 and 13 demonstrate the effectiveness of the automated detuning technique: by disconnecting the electrical load, the mechanical displacement is reduced from 145μm to 58μm (a 60% decrease), effectively protecting the receiver against rapid increases in the magnetic field.

This demonstration confirms that it is possible to implement the proposed MD and MTP modes solely with the knowledge of the piezoelectric voltage, without requiring any information about the magnetic field or the mechanical displacement of the receiver, which would otherwise necessitate power-consuming and bulky sensors. The proposed detuning technique could be integrated into a self-powered circuit that would consume a negligible amount of the transmitted power.

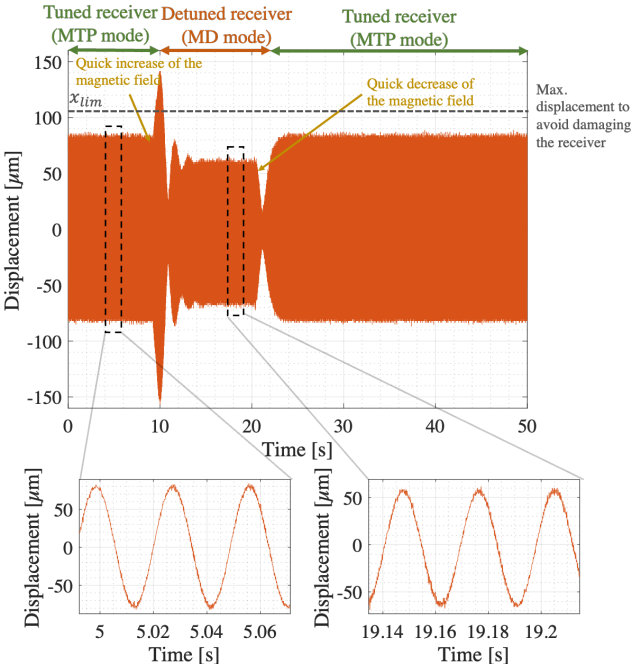

Figure 12 – Experimental run illustrating an abrupt increase in the mechanical displacement of the receiver due to an increased magnetic field. This figure demonstrates the operation of the automated detuning mode which actively protects the electromechanical receiver against excessive increases in mechanical displacement.

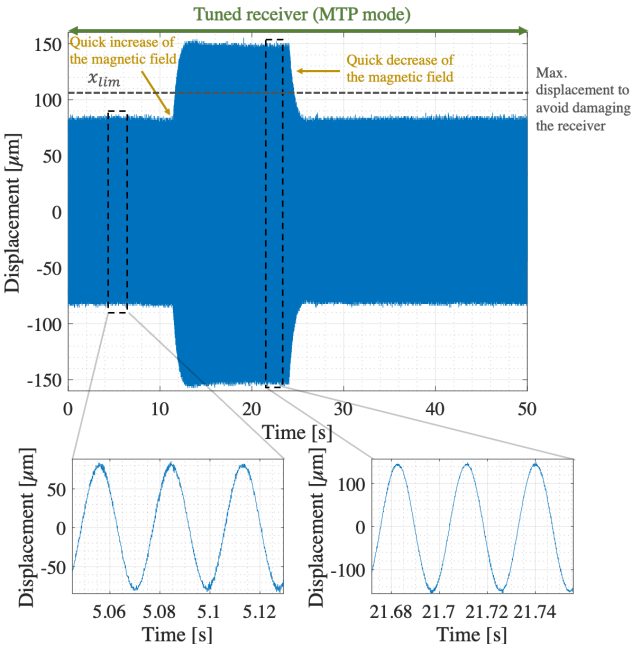

Figure 13 – Experimental run illustrating an abrupt increase in the mechanical displacement of the receiver due to an increased magnetic field. In this run, the detuning mode has been deactivated, showcasing the system's response without the protective detuning mechanism.

Conclusion

This article presents an electrical method for detuning the receiver in EWPT systems. We have developed an analytical model to analyze the impact of the electrical load on the receiver's displacement and derived an expression for the maximum displacement reduction achievable with a specific receiver. This maximum displacement reduction depends solely on the electromechanical coupling and the mechanical quality factor of the receiver. Experimental validation of our models was conducted using a dedicated setup and a custom piezoelectric receiver. The experimentally observed displacement reduction closely aligns with our analytical model predictions.

Furthermore, we introduced an automated algorithm that facilitates the transition between MTP and MD modes, based on the amplitude of the receiver voltage. This detuning algorithm has been successfully implemented on dSpace, which proved effective in reducing displacement by 60% during a sudden increase in the magnetic field. The proposed detuning approach could therefore be used to limit the displacement of the receiver in the event of increased transmitter-receiver coupling due to posture changes or breathing in biomedical applications.

Our next goal is to integrate the proposed electrical detuning algorithm into a dedicated, self-powered circuit. This circuit aims to optimize the power transmitted to the receiver and to automatically detune it in order to prevent damage in the event of an increased magnetic field. Replacing the resistive load tuning/detuning by nonlinear voltage processing inspired from piezoelectric energy harvesting circuits could also enhance the detuning process, with stronger electrically-induced damping, and extend the range of application of the proposed approach (see Appendix B). This advancement promises to significantly enhance the safety and robustness of EWPT systems in applications where coupling variations may occur.

Acknowledgments

The authors received no financial support for the research, authorship, and/or publication of this article.

References

[1] J. Ponmozhi, C. Frias, T. Marques, O. Frazao, “Smart sensors/actuators for biomedical applications: Review,” *Measurement*, vol. 45, no. 7, pp. 1675-1688, 2012.

[2] A. Iqbal, P. R. Sura, M. Al-Hasan, I. B. Mabrouk, T. A. Denidni, “Wireless power transfer system for deep-implaned biomedical devices,” *Nature Scientific Reports* 12, 13689, 2022.

[3] Z. Zhang, H. Pang, A. Georgiadis and C. Cecati, “Wireless Power Transfer—An Overview,” *IEEE Transactions on Industrial Electronics*, vol. 66, no. 2, pp. 1044-1058, Feb. 2019.

[4] M. Schormans, V. Valente and A. Demosthenous, “Practical Inductive Link Design for Biomedical Wireless Power Transfer: A Tutorial,” in *IEEE Transactions on Biomedical Circuits and Systems*, vol. 12, no. 5, pp. 1112-1130, Oct. 2018, doi: 10.1109/TBCAS.2018.2846020.

[5] M. A. Houran, X. Yang, W. Chen, “Magnetically Coupled Resonance WPT: Review of Compensation Topologies, Resonator Structures with Misalignment, and EMI Diagnostics,” *Electronics*, vol. 7, no. 11, 296, 2018.

[6] U.-M. Jow and M. Ghovanloo, “Modeling and Optimization of Printed Spiral Coils in Air, Saline, and Muscle Tissue Environments,” in *IEEE Trans. Biomed. Cir. And Sys.*, vol. 3, no. 5, pp. 339-347, 2009, doi: 10.1109/TBCAS.2009.2025366.

[7] “IEEE Standard for Safety Levels with Respect to Human Exposure to Electric, Magnetic, and Electromagnetic Fields, 0 Hz to 300 GHz,” in *IEEE Std C95.1-2019*, pp.1-312, 4 Oct. 2019, doi: 10.1109/IEEESTD.2019.8859679.

[8] H. Zangl, et al., “Wireless Communication and Power Supply Strategy for Sensor Applications Within Closed Metal Walls,” in *IEEE Transactions on Instrumentation and Measurement*, vol. 59, no. 6, 2010.

[9] O. Saha, B.D. Truong, S. Roundy, “A review of wireless power transfer using magnetoelectric structures,” *Smart Materials and Structures*, vol. 31, no. 11, 113001, 2022.

[10] N. Garraud, *et al*, “Modeling and experimental analysis of rotating magnet receivers for electrodynamic wireless power transmission,” *J. Phys. D: Appl. Phys., vol.* 52, 185501, 2019.

[11] M. A. Halim, A. A. Rendon-Hernandez, S. E. Smith and D. P. Arnold, "Analysis of a Dual-Transduction Receiver for Electrodynamic Wireless Power Transfer," in *IEEE Transactions on Power Electronics*, vol. 37, no. 6, pp. 7470-7479, 2022.

[12] E. Andersen, S. Roundy, B.D. Truong, “Frequency-dependence of power and efficiency for resonant inductive coupling and magnetoelectric wireless power transfer systems,” *Smart Materials and Structures*, vol. 31, 105026, 2022.

[13] D. J. Graham, et al., “Investigation of Methods for Data Communication and Power Delivery Through Metals,” in *IEEE Transactions on Industrial Electronics*, vol. 58, no. 10, pp. 4972-4980, Oct. 2011.

[14] P. Si, A. P. Hu, S. Malpas, D. Budgett, “A Frequency Control Method for Regulating Wireless Power to Implantable Devices,” *IEEE Transactions on Biomedical Circuits and Systems*, vol. 2, no. 1, 2008.

[15] Y.-C. Yen, P.S. Riehl, H. Akram, and A. Satyamoorthy, “Wireless power receiver with programmable path”, *US patent number WO2015105924*, 2015.

[16] M. A. Houran, X. Yang and W. Chen, “Two-Degree-of-Freedom WPT System Using Cylindrical-Joint Structure for Applications With Movable Parts,” in *IEEE Transactions on Circuits and Systems II: Express Briefs*, vol. 68, no. 1, pp. 366-370, 2021.

[17] C. Zhang, D. Lin and S. Y. R. Hui, “Ball-Joint Wireless Power Transfer Systems,” in *IEEE Transactions on Power Electronics*, vol. 33, no. 1, pp. 65-72, 2018.

[18] M. A. Houran, X. Yang and W. Chen, “Design and analysis of coaxial cylindrical WPTcoils for two-degree-of-freedom

applications," *Journal of Physics D: Applied Physics*, vol. 53, no. 49, 495004, 2020.
[19] T. D. Dissanayake et al., "A Novel Low Temperature Transcutaneous Energy Transfer System Suitable for High Power Implantable Medical Devices: Performances and Validation in Sheep," *Artificial organs*, vol. 34, no. 5, 2010.
[20] B. M. Badr, A. Makosinski, N. Dechev, K. R. Delaney, "Controlling wireless power transfer by tuning and detuning resonance of telemetric devices for rodents," *Wireless Power Transfer*, 1-14, 2020.
[21] J. James, J. Boys and G. Covic, "A variable inductor based tuning method for ICPT pickups," *in 7th IEEE IPEC Conference*, pp. 1142–1146, 2005.
[22] J.-U.W. Hsu, A.P. Hu and A. Swain, "A wireless power pickup based on directional tuning control of magnetic amplifier," *IEEE Transactions on Industrial Electronics*, vol. 56, pp. 2771–2781, 2009.
[23] C.-Y. Huang, J. Boys, G. Covic and S. Ren, "LCL pick-up circulating current controller for inductive power transfer systems," *in Energy Conversion Congress and Exposition*, pp. 640–646, 2010.
[24] E. Halvorsen, "Energy Harvesters Driven by Broadband Random Vibrations," *Journal of Microelectromechanical Systems, 17(5),* 2008.
[25] J. M. Renno, M. F. Daqaq, D. J. Inman, "On the optimal energy harvesting from a vibration source," *Journal of Sound and Vibration*, vol. 320, pp. 386-405, 2009.
[26] F. Fiorillo, "Measurement and Characterization of Magnetic Materials" 1st edn (Amsterdam: Elsevier), 2004.
[27] V. R. Challa, et al., "Wireless power transmission to an electromechanical receiver using low-frequency magnetic fields," *Smart Materials and Structures*, vol. 21, 115017, 2012.
[28] Y. Liao and H. A. Sodano, "Model of a single mode energy harvester and properties for optimal power generation," *Smart Materials and Structures,* vol. 17, p. 065026, November 2008.
[29] S. Leadenham, A. Moura, A. Erturk, "Exploiting material softening in hard PZTs for resonant bandwidth enhancement," Proceedings Volume 9799, Active and Passive Smart Structures and Integrated Systems, 2016.
[30] J. Liang and W.-H. Liao, "Impedance Modeling and Analysis for Piezoelectric Energy Harvesting Systems," *IEEE/ASME Transactions on Mechatronics,* vol. 17, no. 6, pp. 1145-1157, December 2012.
[31] R. D'hulst, T. Sterken, R. Puers, G. Deconinck and J. Driesen, "Power Processing Circuits for Piezoelectric Vibration-Based Energy Harvesters," in *IEEE Transactions on Industrial Electronics*, vol. 57, no. 12, pp. 4170-4177, Dec. 2010, doi: 10.1109/TIE.2010.2044126.
[32] Y. Liao and J. Liang, "Maximum power, optimal load, and impedance analysis of piezoelectric vibation energy harvesters," *Smart Materials and Structures*, vol. 27, no. 7, 075053, 2018.
[33] A. Morel et al., "Resistive and reactive loads' influences on highly coupled piezoelectric generators for wideband vibrations energy harvesting," *Journal of Intelligent Material Systems and Structures*, vol. 30, no. 3, pp. 386-399, 2019.
[34] S. R. Anton, A. Erturk, D. J. Inman, "Bending Strength of Piezoelectric Ceramics and Single Crystals for Multifunctional Load-Bearing Applications," *IEEE Transactions on Ultrasonics, Ferroelectrics, and Frequency control,* vol. 59, no. 6, 2012.
[35] N. Chen, P. Yan, J. Ouyang, "A Generalized Approach on Bending and Stress Analysis of Beams with Piezoelectric Material Bonded," *Sensors and Actuators A: Physical*, vol. 290, pp. 54-61, 2019.
[36] P.V. Avvari, Y. Yang, C. K. Soh, "Long-term fatigue behavior of a cantilever piezoelectric energy harvester", *Journal of Intelligent Material Systems and Structures*, vol. 28, no. 9, 2016.
[37] D. Gibus, et al., "Strongly coupled piezoelectric cantilevers for broadband vibration energy harvesting," *Applied Energy*, vol. 277, 115518, 2020.
[38] Y. Kuang, Z.J. Chew, M. Zhu, "Strongly coupled piezoelectric energy harvesters: Finite element modelling and experimental validation," *Energy Conversion and Management*, vol. 213, 112855, 2020.
[39] A. Morel, G. Pillonnet, Y. Wanderoild, A. Badel, "Dielectric losses considerations for piezoelectric energy harvesting," *Journal of Low Power Electronics*, vol. 14, no. 2, pp. 244-254, 2018.
[40] A. Badel, E. Lefeuvre, "Nonlinear conditioning circuits for piezoelectric energy harvesters," *Springer International Publishing,* in Nonlinearity in Energy Harvesting systems, vol. 25, no. 2, 2016.
[41] A. Brenes, A. Morel, J. Juillard, E. Lefeuvre, A. Badel, "Maximum power point of piezoelectric energy harvesters: a review of optimality condition for electrical tuning," *Smart Materials and Structures*, vol. 29, 033001, 2020.

Appendix A – Expression for the resonant frequency of the electromechanical receiver

As demonstrated in [41], the optimal frequency that maximizes the transmitted power can be found by solving (27):

$$1 - \Omega_{res}^2 + k_m^2 U_p(\Omega_{res}) = 0 \tag{27}$$

With $U_p(\Omega_{res}) = \frac{(r\Omega_{res})^2}{1+(r\Omega_{res})^2}$ representing the voltage term in-phase with mechanical displacement. Consequently, this leads to equation (28) which can be solved to find the expression for Ω_{res}.

$$1 - \Omega_{res}^2 + \frac{k_m^2\,(r\Omega_{res})^2}{1 + (r\Omega_{res})^2} = 0 \tag{28}$$

Solving equation (28) provides the expression for the optimal frequency of the electromechanical receiver, Ω_{res}:

$$\Omega_{res} = \frac{1}{r}\sqrt{\frac{(r^2(1+k_m^2)-1)+\sqrt{(r^2(1+k_m^2)-1)^2+4r^2}}{2}} \quad (29)$$

Appendix B – Magnetic field range for electrical detuning

This appendix assesses the magnetic field range within which the proposed detuning technique can be effectively applied for a given application. From equations (5) and (16), the magnetic field that can be tolerated by a given receiver without detuning is given by:

$$B(l) \leq \frac{\sqrt{2}\,\mu_0}{Q\,V\,B_r}\Omega_m\,K\,L_b x_{m,lim} \quad (30)$$

From equation (19), the proposed detuning technique can ensure that the minimum displacement amplitude remains smaller than the displacement limit only if the following condition is satisfied:

$$x_{m_{opt}} \leq \frac{\sqrt{(k_m^2 Q)^2+1}}{2} x_{m,lim} \quad (31)$$

Combining (30) with (31) leads to the following condition on the magnetic field at the receiver's location in case of electrical detuning:

$$B(l) \leq \frac{\sqrt{2}\,\mu_0}{Q\,V\,B_r}\Omega_m\,K\,L_b\frac{\sqrt{(k_m^2 Q)^2+1}}{2} x_{m,lim} \quad (32)$$

Therefore, the proposed electrical detuning allows reaching magnetic field levels that are $\frac{\sqrt{(k_m^2 Q)^2+1}}{2}$ times more significant than without detuning, in order to avoid breaking the receiver. In the case (32) cannot be met, the proposed detuning approach cannot be employed to maintain $x < x_{m,lim}$. This underscores the importance of maximizing the electromechanical coupling of the receiver in order to enhance the applicability of the proposed electrical detuning approach.

Appendix C – Combining maximum power and detuning mode

This appendix investigates a combined MD-MTP mode, aiming to maximize transmitted power while adequately detuning the receiver to satisfy the condition $x_m = x_{m,lim}$. From equation (17), this condition can be rewritten as (33), considering $\Omega_m = 1$ (case 1).

$$\frac{2x_{m_{opt}}/Q}{\sqrt{\left(\frac{k_m^2\, r_{opt}^2}{1+r_{opt}^2}\right)^2+\left(\frac{1}{Q}+\frac{k_m^2\, r_{opt}}{1+r_{opt}^2}\right)^2}} = x_{m,lim} \quad (33)$$

From (33), the expression of the optimal resistance r_{opt} can be obtained.

$$r_{opt} = \frac{\sqrt{-\frac{x_{m,lim}^4}{16x_{m_{opt}}^4}+\frac{x_{m,lim}^2}{4x_{m_{opt}}^2}(2+(k_m^2Q)^2)-1-\frac{x_{m,lim}^2}{4x_{m_{opt}}^2}Qk_m^2}}{\frac{x_{m,lim}^2}{4x_{m_{opt}}^2}(1+(k_m^2Q)^2)-1} \quad (34)$$

Note that r_{opt} only exists if $\frac{x_{m,lim}}{x_{m_{opt}}} \geq 2/\sqrt{(k_m^2Q)^2+1}$, as detailed by (19). Combining (34) with (12) leads to the expression for maximized transmitted power in the case of a detuned receiver.

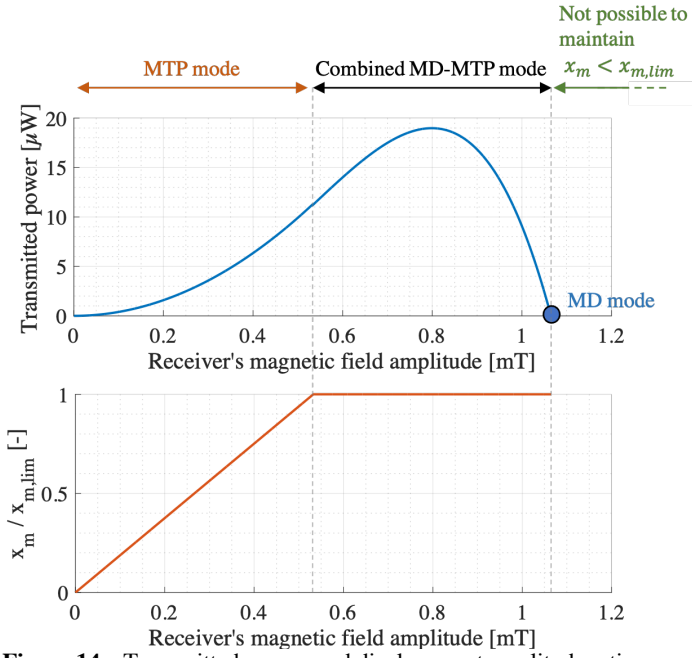

Figure 14 – Transmitted power and displacement amplitude ratio as a function of the receiver's magnetic field amplitude, for $k_m^2 = 0.046$, $Q = 131$, and $x_{m,lim} = 100\mu m$.

Figure 14 illustrates the evolution of transmitted power as a function of receiver's magnetic field amplitude. For weak magnetic fields (when $x_m < x_{m,lim}$), the receiver operates in MTP mode. Since maximum power is a function of the squared magnetic field (6), the transmitted power increases with B^2. For larger magnetic fields, when the displacement amplitude of the inertial mass reaches $x_{m,lim}$, the system operates in combined MD-MTP mode, where displacement is constrained to $x_{m,lim}$. In this mode, the power increases for slightly larger B (but at a slower rate than B^2) and then starts

to decrease as the required detuning becomes too significant ($B > 0.8mT$). Eventually, with further increase in the magnetic field, the system operates in MD mode. In this case, the detuning is maximized, implying that no power can be transmitted. For even larger magnetic fields, the proposed detuning scheme cannot ensure $x_m \leq x_{m,lim}$, posing a risk of damaging the receiver.

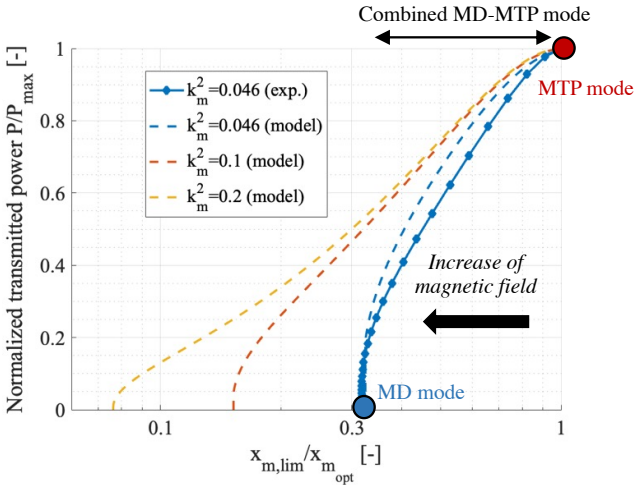

Figure 15 – Normalized power P/P_{max} as a function of displacement ratio $x_{m,lim}/x_{m_{opt}}$, for three electromechanical coupling values k_m^2, and $Q = 131$. Experimental results have been obtained with the prototype shown in Fig.8.

Figure 15 presents a broader dimensionless view of the evolution of transmitted power in the combined MD-MTP mode, along with the displacement ratio $x_{m,lim}/x_{m_{opt}}$. As the magnetic field increases, the optimal displacement amplitude $x_{m_{opt}}$ increases, leading to a decrease in the displacement ratio. Since the maximum power P_{max} also increases with stronger magnetic fields ($\propto B^2$), the ratio of transmitted power over maximum power decreases with increased detuning. One may note that, for a given displacement ratio $x_{m,lim}/x_{m_{opt}}$, the reduction in transmitted power is less significant for receiver with stronger electromechanical coupling.